Nano Research

Open Access

Research Article

Synergistic fibrillization engineering in donor and acceptor phases enables high-performance all-polymer solar cells

Bin Zhang[1] ✉, Yushou Zhao[1], Xiaofeng Qin[1], Aiqin Li[1], Xinling Li[1], Wenming Li[1], Weile Guo[1], Xiaolan Qin[1], Zhicai He[3], Yong Hua[4], Menglan Lv[1] ✉, and Liming Ding[2] ✉

[1] *Engineering Research Center for Energy Conversion and Storage Technology of Guizhou, School of Chemistry and Chemical Engineering, Guizhou University, Guiyang 550025, China*
[2] *School of Chemical Engineering and Light Industry, Guangdong University of Technology, Guangzhou 510006, China*
[3] *Institute of Polymer Optoelectronic Materials and Devices, State Key Laboratory of Luminescent Materials and Devices, South China University of Technology, Guangzhou 510640, China*
[4] *School of Materials and Energy, Yunnan University, Kunming 650091, China*

Cite this article: *Nano Research*, **2025**, *18*, 94907295. https://doi.org/10.26599/NR.2025.94907295

ABSTRACT: Recently, all-polymer solar cells (all-PSCs) have become an important organic photovoltaic technology, ascribing to their unique characteristics of high stability and mechanical endurance. However, the morphology control between polymer donor and polymer acceptor suffers from tough difficulties, resulting from the nature of rigid planarity and chain entanglement in the conjugated polymer backbones. In this work, we utilize an additive, 1-chloro-naphthalene (CN), to regulate polymer chain stacking and orientation in D18:PY-IT system, resulting in the formation of versatile nano-scale polymer fibrillization between donor and acceptor phases. Consequently, the CN-modified D18:PY-IT blend film shows improved molecular stacking characteristics and distinct nano-scale bi-continuous phase separation. Attributing to the incorporation of CN additive in a bulk-heterojunction (BHJ) D18:PY-IT system, it exhibits higher photovoltaic performance than the as-cast and only thermal annealing (TA) treated devices, where the CN-based device provides a power conversion efficiency (PCE) of 17.31%, an open-circuit voltage (V_{OC}) of 0.955 V, a short-circuit current density (J_{SC}) of 24.16 mA·cm^{-2}, and a fill factor (FF) of 74.99%, respectively. This is one of the highest photovoltaic performances reported in the D18:PY-IT based binary BHJ all-PSCs. Hence, it is evident that the morphology in all-PSCs can be feasibly modulated via incorporating appropriate additive into active layer for achieving excellent photovoltaic performance.

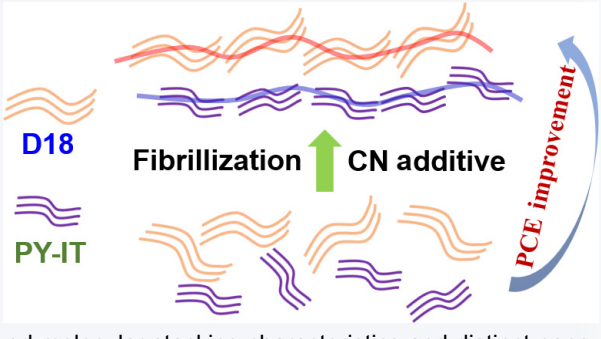

KEYWORDS: fibrillization engineering, morphology control, additive, 1-chloro-naphthalene, all-polymer solar cells

1 Introduction

Polymer solar cells (PSCs), as an emerging new photovoltaic technology, have become a hot issue both academically and commercially, resulting from their merits in low cost, light weight, feasible functionalization, and large-scale solution processibility [1]. Owing to the recent tremendous efforts in materials development and device engineering, the power conversion efficiencies (PCEs) in PSCs have exceeded to 20% [2–5]. This achievement sheds impressive light on the potential commercialization of PSCs as a competing photovoltaic technology in the future.

In PSCs, it is widely established that they generally exhibit the sandwiched device structure, comprising of anode, hole transport layer (HTL), active layer, electron transport layer (ETL), and cathode [6]. Even though the HTL and ETL are very important functional layers, the active layer also plays a pivotal role in determining photovoltaic performance in PSCs [7]. It means that the excellent active layers can realize high PCEs and stability. Usually, the active layer includes the donor and acceptor materials, where the donor works as an electron-donating unit and acceptor plays a role of electron-accepting function [8]. In the donors, the widely used ones are semiconducting p-typed polymers, such as D18 [9–11] and PM6 [12]. Whereas, the acceptors are typically

Received: November 26, 2024; **Revised:** January 15, 2025
Accepted: February 10, 2025

✉Address correspondence to Bin Zhang, zhangb@gzu.edu.cn; Menglan Lv, mllv@gzu.edu.cn; Liming Ding, ding@nanoctr.cn

selected as small molecules such as 2,2'-((2Z,2'Z)-((12,13-bis(2-ethylhexyl)-3,9-diundecyl-12,13-dihydro-[1,2,5]thiadiazolo[3,4-e]thieno[2',3':4',5']thieno[3,2,3':4,5]pyrrolo[3,2-g]thieno[2',3':4,5]thieno[3,2-b]indole-2,10-diyl)bis(methylene))bis(5,6-difluoro-3-oxo-2,3-dihydro-1H-indene-2,1-diylidene))dimalononitrile) (Y6) [13], 2,2'-((2Z,2'Z)-((3,9-bis(2-butyloctyl)-12,13-bis(2-ethylhexyl)-12,13-dihydro-[1,2,5]thiadiazolo[3,4-e]thieno[2",3":4',5']thieno[2',3':4,5]pyrrolo[3,2-g]thieno[2',3':4,5]thieno[3,2-b]indole-2,10-diyl)bis(methaneylylidene))bis(5,6-difluoro-3-oxo-2,3-dihydro-1H-indene-2,1-diylidene))dimalononitrile (L8-BO) [14], and 2,2'-((2Z,2'Z)-((12,13-bis(2-butyloctyl)-3,9-dinonyl-12,13-dihydro-[1,2,5]thiadiazolo[3,4-e]thieno[2",3":4',5']thieno[2',3':4,5]pyrrolo[3,2-g]thieno[2',3':4,5]thieno[3,2-b]indole-2,10-diyl)bis(methaneylylidene))bis(5,6-dichloro-3-oxo-2,3-dihydro-1H-indene-2,1-diylidene))dimalononitrile (BTP-eC9) [15], and polymers such as PYT [16], PY-IT [17], and their derivatives [18–20]. Through the optimization on blend films of these donors and acceptors, the bulk-heterojunction (BHJ) active layer is formed, leading to the highly photovoltaic properties.

On the basis of recent studies, the polymer donor and small-molecule acceptor systems can give highly photovoltaic performance, including D18:Y6, D18:L8-BO, and PM6:L8-BO systems [21]. Although these high achievements in polymer/small molecule systems are realized, they also suffer from the obvious difficulties of obtaining excellent PSCs, for instance, the device stability and mechanical endurance. In small-molecule-based PSCs, the small molecular acceptor might tend to aggregate each other, forming large-scale phase separation between donor and acceptor phases during long-term operation, which would make charge recombination at the phase interface seriously and is very detrimental for visualizing highly stable PSCs. On the other hand, the polymer:polymer system, denoted as all-PSCs, emerged and developed, where both donor and acceptor materials are all polymers [22, 23]. In all-PSCs, ascribing to the rigid backbone and long chains of polymers, the nano-scale phase separation would be more stable to suppress negative molecular aggregation in BHJ active layer, leading to long-time stability and mechanical endurance. When all-PSCs have been developed as an alternative device in organic photovoltaics, the efficiencies are catching up with the small-molecule-based PSCs, indicating that all-PSCs are potentially a useful and promising photovoltaic technology [24–26].

Even though all-PSCs have gotten a great success, they also encounter the difficulties in morphology control of active layer, originating from the existence of wriggling in rigid and long-chain polymer backbones. These polymer backbones would weaken chain moving and hinder nano-scale and bi-continuous phase separation, resulting in the phases mixing or extremely large-scale phase separation [27]. Previously, some of methods have been adopted to conquer this difficulty, for example, thermal annealing (TA) [28], addition of solvent [29] and solid additives [30, 31], and layer-by-layer process [32]. However, it is still a problem to form the ideal phase separation between polymer donor and polymer acceptor. It is believed that the better dual-phases fibrillization in polymer donor and polymer acceptor, the better morphology formation [33]. This improved polymeric fibrillization can strengthen the molecular stacking and enhance the charge transport in the active layer, lowering charge recombination and energy loss effectively. Therefore, to facilitate morphology modulation and acquire highly photovoltaic performance, it is urgent to investigate phase separation and polymer fibrillization in all-PSCs detailedly.

In this work, an all-PSC is developed and investigated, where a star-of-the-art p-typed polymer of D18 is selected as donor material and an n-typed polymer of PY-IT is used as acceptor material. To control and optimize the morphologies, an additive of 1-chloronaphthalene (CN) is introduced to D18:PY-IT blend film. Attributing to the introduction of CN, the phases of D18:PY-IT are controlled greatly, resulting in the formation of excellent nano-scale polymeric fibrils. This fibrillization process is beneficial for the dual-phases separation, which would improve exciton diffusion and separation, and thereby suppress charge recombination. As a result, a higher PCE of 17.31% with an open-circuit voltage (V_{OC}) of 0.955 V, a short-circuit current density (J_{SC}) of 24.16 mA·cm^{-2}, and a fill factor (FF) of 74.99% is achieved, rather than those of control devices without additive and with only thermal annealing. To the best of our knowledge, this PCE is one of the highest values reported in D18:PY-IT based binary BHJ all-PSCs. Hence, it is demonstrated that the introduction of appropriate additives is a promising and effective methodology to control all-polymer phases for forming great fibril networks in all-PSCs.

2 Results and discussion

2.1 Optical properties

As presented in Fig. 1(a), the chemical structures of D18, PY-IT, and CN were shown in detail. To get the optical properties of polymer donor and acceptor, the ultraviolet–visible (UV–vis) absorption and photoluminescence (PL) tests were carried out, as shown in Figs. 1(b) and 1(c). It is noted that the D18 and PY-IT exhibit a complementary absorption, showing a wide responsive range from 300 to 850 nm. To investigate the energy transfer between D18 donor and PY-IT acceptor, the PL measurement was performed, as presented in Fig. 1(c). It is apparent that when PY-IT is introduced to form D18:PY-IT blend film, the PL of D18 is quenched obviously, indicating that the energy excited from D18 is transferred to PY-IT feasibly [34]. To further study the additive influence on energy transfer from D18 to PY-IT, the PL measurement of different blend films was also performed, as shown in Fig. S1 in the Electronic Supplementary Material (ESM). It illustrates that when CN is introduced as a solvent additive, the PL intensity is reduced more greatly than the control blend film without additive. This decreased PL implies that CN can make the energy transfer from D18 to PY-IT more sufficiently, which is potentially beneficial for realizing highly photovoltaic performance in all-PSCs.

2.2 Photovoltaic performance

To investigate the additive influence on photovoltaic performance, a conventional device structure of indium-tin oxide (ITO)/poly(3,4-ethylenedioxythiophene):polystyrenesulfonic acid (PEDOT:PSS)/D18:PY-IT/2,9-bis(3-((3-(dimethylamino)propyl)amino)propyl)anthra[2,1,9-def:6,5,10-d'e'f']diisoquinoline-1,3,8,10(2H,9H)-tetraone (PDINN)/Ag was utilized, as presented in Fig. 2(a), and the corresponding energy level was shown in Fig. 2(b). In Fig. 2(c), the current density–voltage (J–V) curves were presented for the devices without additive, with only TA, and with CN treatment, respectively. To find out the best ratio of CN additive in blend film, the variation effect of additive ratio on photovoltaic performance was also studied, as shown in Fig. S2 and Table S1 in the ESM. It is noted that the device without CN additive gives a photovoltaic performance with a V_{OC} of 0.947 V, a J_{SC} of 23.51 mA·cm^{-2}, an FF of

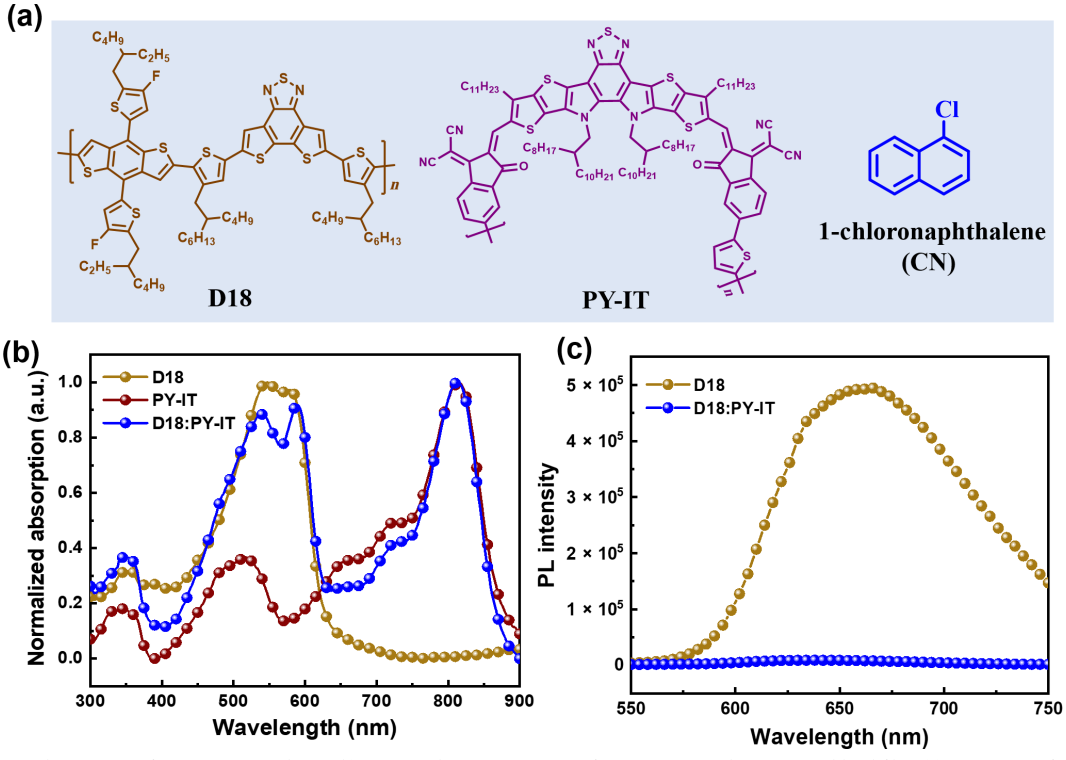

Figure 1 (a) Chemical structures of D18, PY-IT, and CN. (b) UV–vis absorption spectra of D18, PY-IT, and D18:PY-IT blend film. (c) PL spectra of D18 and D18:PY-IT blend film.

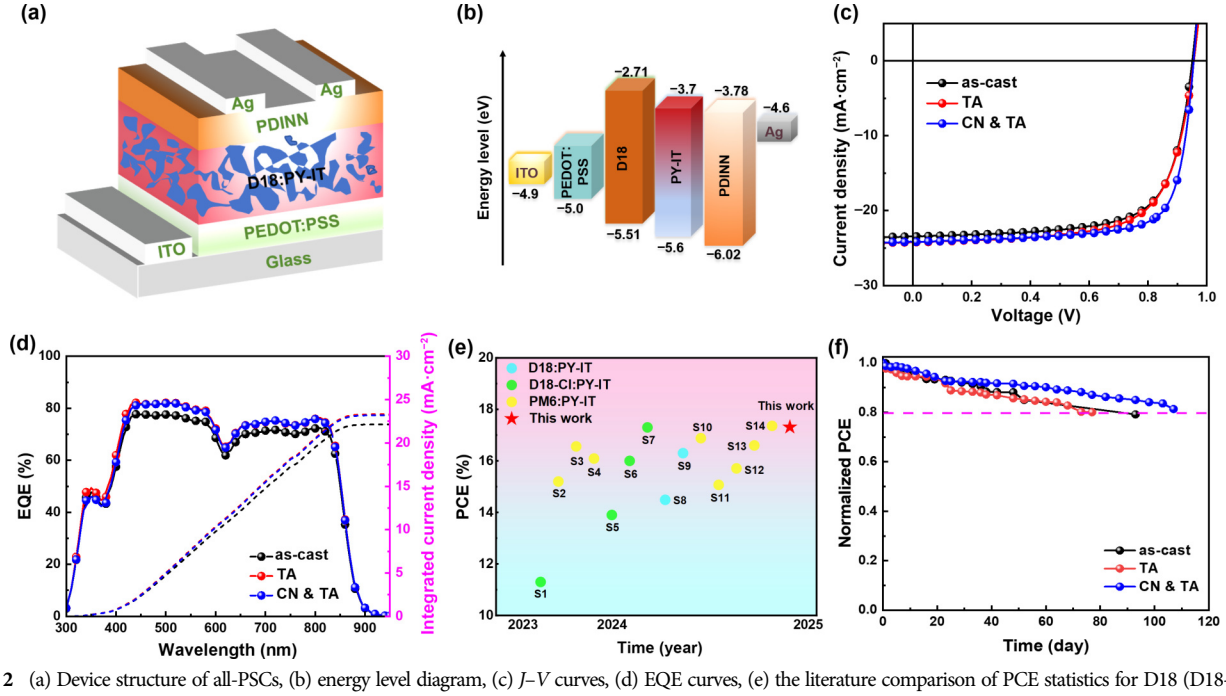

Figure 2 (a) Device structure of all-PSCs, (b) energy level diagram, (c) *J*–*V* curves, (d) EQE curves, (e) the literature comparison of PCE statistics for D18 (D18-Cl and PM6):PY-IT based binary BHJ all-PSCs, the S1–S14 are supported in Table S3 in the ESM, and the red star represents the photovoltaic performance of D18:PY-IT in this work, and (f) storage lifetimes of devices without encapsulation in N_2.

69.33%, and a PCE of 15.43%, respectively. When the device is treated with only TA, the photovoltaic performance is improved slightly, which indicates that the TA would not influence on device performance dramatically. Surprisingly, the photovoltaic performance is improved obviously when CN additive is introduced to D18:PY-IT system, where it provides a high PCE of 17.31% with a V_{OC} of 0.955 V, a J_{SC} of 24.16 mA·cm^{-2}, and an FF of 74.99%, respectively. This enhancement in photovoltaic performance is mainly attributed to the improvement in FF value, possibly resulting from the optimization of phase separation between polymer donor and polymer acceptor. As presented in Fig. 2(d), it showed the external quantum efficiency (EQE) curves of devices. It is noted that all devices exhibit broad light-responsive range from 300 to 850 nm, implying that these devices realize the

efficient photo-to-current conversion. Also, the integrated J_{SC} values, as presented in Table 1, are consistent with the values from *J*–*V* curves. To further explore the D18:PY-IT system with CN additive penetratingly, the thickness effect of active layer on photovoltaic performance was investigated, as presented in Fig. S3 in the ESM, and the device performance was summarized in Table S2 in the ESM. It is found that D18:PY-IT system with CN additive also shows a high photovoltaic performance even at different thicknesses of D18:PY-IT films, where it even provides a PCE of 14.73% at a 300 nm-thick active layer, keeping 85% efficiency of the initial PCE [35]. This result illustrates that D18:PY-IT system can give the high photovoltaic performance at thick active layer, which is beneficial for compatibility with the large-scale roll-to-roll process in the future [36]. To the best of our knowledge, this 17.31% efficiency is one of the best PCEs based on the reported D18 (or D18-Cl):PY-IT binary BHJ systems, as presented in Fig. 2(e) and Table S3 in the ESM. To study the device stability, the storage lifetimes of devices without encapsulation in N_2 were tested, as shown in Fig. 2(f). It is illustrated that all devices display high stability, where the CN-treated device gives the highest stability with a T_{80} lifetime of more than 100 days (T_{80} IS the time of which the PCE decreases to 80% of its initial value). To further evaluate the thermal stability, the photovoltaic performance of unencapsulated devices was tested at 65 °C, as presented in Fig. S4 in the ESM. It shows that all of devices have high thermal stability, and the PCEs can keep more than 80% of the initial values after the continuous heating for 300 h; but the CN-based device exhibits the better thermal stability than other two control devices. These findings demonstrate that the introduction of CN additive in D18:PY-IT system not only improves efficiency but also enhances device stability spontaneously.

2.3 Morphology properties

To study the molecular stacking characteristics and crystallinity, the grazing incidence wide angle X-ray scattering (GIWAXS) was employed for testing both pristine polymers and blend films, respectively [37]. Preliminarily, the GIWAXS test for pristine D18 and PY-IT were carried out in detail, as presented in Fig. 3, and the related data were summarized in Tables S4 and S5 in the ESM. For neat D18 film, it is found that the introduction of CN is preferable to forming the face-on orientation, demonstrated by the evidence that the CN-modified D18 film shows stronger (010) diffraction peaks of 1.686 $Å^{-1}$ in out-of-plane (OOP) direction than other two control films of as-cast (1.665 $Å^{-1}$) and TA (1.672 $Å^{-1}$) treatment. Accordingly, the CN-based D18 film also exhibits higher lamellar (100) stacking peaks in in-plane (IP) direction at 0.308 $Å^{-1}$ than those of as-cast (0.301 $Å^{-1}$) and TA (0.306 $Å^{-1}$) treated neat D18 films. The crystal coherence length (CCL) values are calculated via Scherrer equation of CCL = 2π × 0.89/full width half maximum (FWHM) to evaluate molecular π–π stacking degree. It is found that when CN is introduced as additive, the CCL value for the (010) diffraction in OOP direction is improved to 24.166 Å, which is higher than the as-cast film of 18.912 Å and TA treatment of 22.003 Å, which indicates that the incorporation of CN allows for better crystalline quality [38]. Similarly, CN can improve the PY-IT neat film to adopt the face-on orientation with the increased CCL values, as presented in Table S5 in the ESM, implying that CN also endows PY-IT with a better molecular stacking and crystallinity.

To further understand the morphology modulation by CN systematically, we investigated the GIWAXS test of binary blend films based on D18:PY-IT, as presented in Fig. 4(a), and the corresponding analyses were summarized in Table S6 in the ESM. It is illustrated that both the (010) diffraction peaks in OOP and the lamellar (100) stacking in IP directions are strengthened distinctly, where the diffraction peaks in OOP are increased from the as-cast film of 1.664 $Å^{-1}$ and TA-treated film of 1.673 $Å^{-1}$ to the CN-optimized film of 1.676 $Å^{-1}$, accompanied by the enhancement on CCLs from 21.490, 24.258, to 25.575 Å for as-cast, TA, and CN treated blend films, respectively. This improved molecular stacking

Table 1 The summary of photovoltaic performance based on D18:PY-IT under AM 1.5 G ($J_{SC}^{integrated}$ is the integrated short-circuit current density from EQE curves)

Devices	V_{OC} (V)	J_{SC} (mA·cm^{-2})	$J_{SC}^{integrated}$ (mA·cm^{-2})	FF (%)	PCE (%)
As-cast	0.947 (0.948 ± 0.006)	23.51 (23.31 ± 0.35)	22.17	69.33 (68.86 ± 0.66)	15.43 (15.22 ± 0.15)
TA	0.945 (0.949 ± 0.004)	24.56 (24.13 ± 0.47)	23.34	68.57 (68.66 ± 0.72)	15.91 (15.72 ± 0.14)
CN & TA	0.955 (0.949 ± 0.006)	24.16 (24.36 ± 0.34)	23.22	74.99 (74.36 ± 0.61)	17.31 (17.19 ± 0.11)

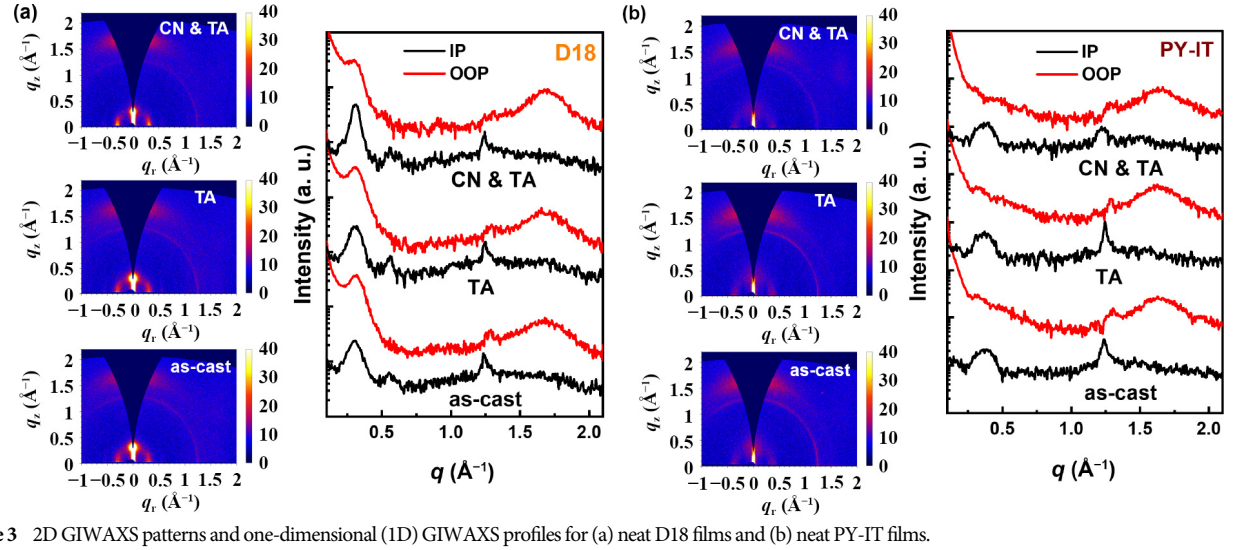

Figure 3 2D GIWAXS patterns and one-dimensional (1D) GIWAXS profiles for (a) neat D18 films and (b) neat PY-IT films.

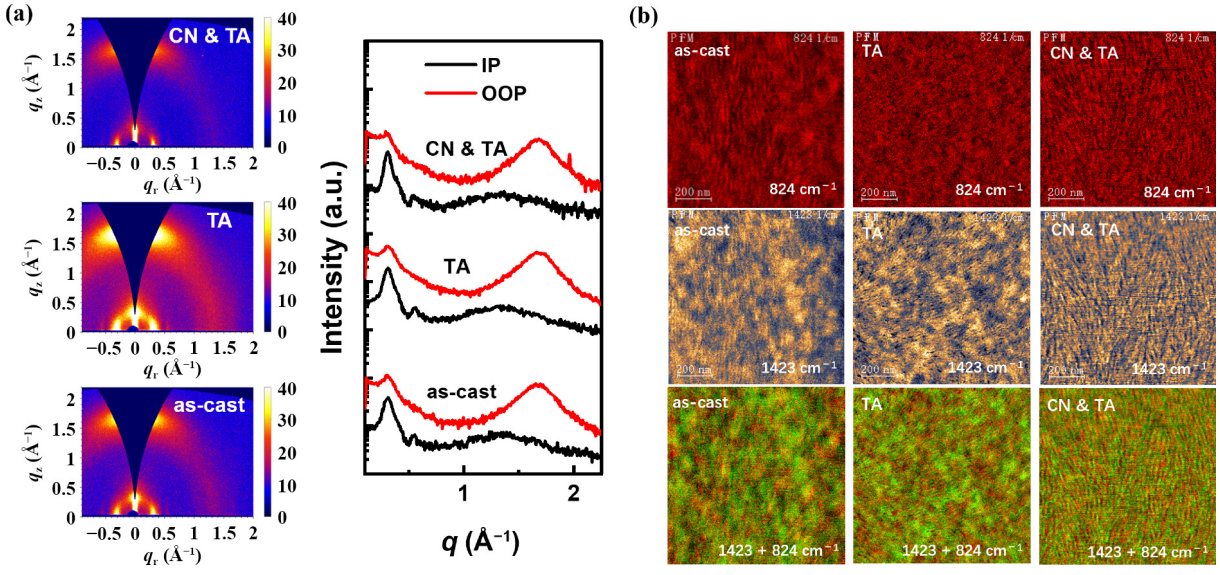

Figure 4 (a) 2D GIWAXS patterns and 1D GIWAXS profiles for D18:PY-IT blend films. (b) PiFM images for D18:PY-IT blend films, where a wave number of 824 cm^{-1} represents D18 and 1423 cm^{-1} represents PY-IT.

can be reflected from atomic force microscope (AFM) test, as displayed in Fig. S5 in the ESM. It is clear that the root-mean roughness (RMS) of as-cast, TA-treated, and CN-treated films are 1.37, 1.33, and 3.9 nm, respectively, which means that the introduction of CN can form good phase separation between donor and acceptor phases. In addition, the AFM images show that the blend films provide the distinct polymer fibrils, as well. These results reveal that the incorporation of CN additive can improve the molecular stacking and crystallinity, benefiting for forming excellent donor and acceptor phases synergistically. Base on the above investigation on GIWAXS tests, we can see that CN optimizes molecular stacking effectively, which is potentially conducive to polymer crystallization for forming advantageous fibrils among polymer donor and polymer acceptor. Hence, to validate the CN additive influence on morphologies, the photoinduced force microscope (PiFM) test at infrared (IR) absorption was carried out to assess the donor and acceptor phase separation, as presented in Fig. 4(b) [39, 40]. Here, the IR wavenumbers at 824 and 1423 cm^{-1} represent D18 and PY-IT, respectively. From Fig. 4(b), it is noted that both D18 and PY-IT in CN-based film show the obvious polymeric fibrils, which implies that they provide excellent molecular stacking and ordering patterns. But the blend films based on as-cast and TA treatment display much phase mixing between polymer donor and polymer acceptor, which would reduce the corresponding phase purities, leading to the stronger charge recombination. In contrast, the blend film with CN additive gives the distinctly continuous dual-phase separation. As a result, this good phase separation scales up each phase's purities between polymer donor and polymer acceptor domains, resulting in better exciton diffusion and charge transport in the active layer. To elucidate the charge transport properties, the electron and hole mobilities were characterized in detail, as presented in Fig. S6 in the ESM. Through calculation, the hole mobilities are improved from 1.97×10^{-4} $cm^2 \cdot V^{-1} \cdot s^{-1}$ of as-cast film and 2.56×10^{-4} $cm^2 \cdot V^{-1} \cdot s^{-1}$ of TA-treated film to 3.92×10^{-4} $cm^2 \cdot V^{-1} \cdot s^{-1}$ of CN-treated film, respectively, whereas the electron mobilities are also enhanced from 1.58×10^{-4} $cm^2 \cdot V^{-1} \cdot s^{-1}$ of as-cast film and 1.42×10^{-4} $cm^2 \cdot V^{-1} \cdot s^{-1}$ of TA-treated film to 1.72×10^{-4} $cm^2 \cdot V^{-1} \cdot s^{-1}$ of CN-treated film, respectively. These results imply that the introduction of CN additive can efficiently optimize the charge transport performance in D18:PY-IT blend film. Overall, the incorporation of CN as additive for D18:PY-IT based active layer can improve the intermolecular stacking and crystallization for forming versatile polymeric fibrils, and optimize phase separation between donor and acceptor, which is beneficial for acquiring highly photovoltaic performance in all-PSCs.

2.4 Charge carrier dynamics

To investigate the effect of additive on exciton dissociation, the relationship of photogenerated current density (J_{ph}) depending on effective voltage (V_{eff}) was studied, as presented in Fig. 5(a). It shows that the photogenerated current densities can be saturated (J_{sat}) at high V_{eff}, implying that the exciton is dissociated and collected completely for all devices. In order to analyze the exciton dissociation quantitatively, the exciton dissociation rates ($\eta_{diss} = J_{ph}^{SC}/J_{sat}$, where J_{ph}^{SC} represents the photogenerated current density) are calculated, depicting that the η_{diss} values are improved from 93.6% of as-cast and 93% of TA-treated devices to 96.7% of CN-treated device, respectively. This enhanced η_{diss} value illustrates that CN can elevate the exciton dissociation in D18:PY-IT-based all-PSCs, leading to higher FF and J_{SC}. To further explore charge carrier dynamics, the J–V curves in the dark were tested, as shown in Fig. 5(b). In contrast to the devices via as-cast process without any treatment and only TA treatment, the device with CN additive provides the lowest reverse saturation current density and the best rectification ratio, ascribing to the optimized phase morphology between donor and acceptor. This enhancement of electric performance in the dark indicates that the device with CN additive exhibits the best charge transport, leading to the best photovoltaic performance. It is widely known that the charge carrier recombination is an indispensable process in PSCs, which is very detrimental to photovoltaic performance, leading to low FF, V_{OC}, J_{SC}, and PCE. Hence, the effective suppression of charge carrier recombination is becoming a significant issue in all-PSCs. Here, the relationships between V_{OC} (or J_{SC}) and light intensity were explored in detail, as presented in Figs. 5(c) and 5(d) [41, 42]. In Fig. 5(c), it

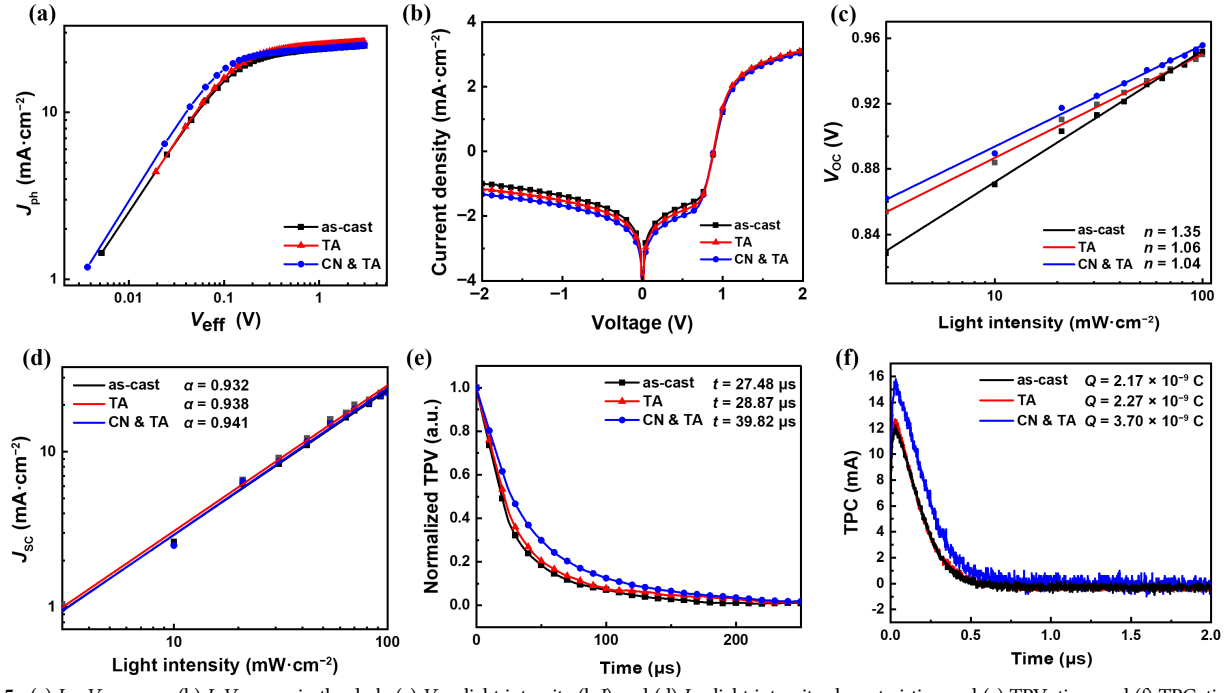

Figure 5 (a) J_{ph}–V_{eff} curves, (b) J–V curves in the dark, (c) V_{OC}–light intensity (ln$I$) and (d) J_{SC}–light intensity characteristics, and (e) TPV–time and (f) TPC–time tests for charge carrier dynamics analysis.

shows the curves of V_{OC}–light intensity relationship, in which the linear slopes of devices with as-cast, TA, and CN treatments are 1.35kT/q (where k, T, and q represent the Boltzmann constant, Kelvin temperature, and elementary charge, respectively), 1.06kT/q, and 1.04kT/q, respectively. It is apparent that the CN-modified device displays the lowest slope than the other two devices, which indicates that the CN additive can reduce the trap-assisted recombination and ultimately enhance the charge transport and collection [43]. Additionally, the relationship between J_{SC} and light intensity was also investigated to explore the influence of additive on bimolecular recombination, as presented in Fig. 5(d). It is known that this relationship is fitted as a linear curve and obeyed the empirical formula of $J_{SC} \propto I^{\alpha}$, where I is light intensity and α value represents the degree of bimolecular recombination. If the α value is 1, it means that there is no bimolecular recombination in all-PSCs. As illustrated in Fig. 5(d), the α values for as-cast, TA, and CN treated devices are 0.932, 0.938, and 0.941, respectively, where the α value of CN-based device is much closer to 1, suggesting that CN can suppress the bimolecular recombination more efficiently and thereby realize lower energy loss and higher photovoltaic performance [44].

To understand the internal charge transport dynamics penetratingly, the transient photovoltage (TPV) and transient-photocurrent (TPC) tests were employed, as presented in Figs. 5(e) and 5(f) [45–47]. From Fig. 5(e), it gives the TPV test with the charge recombination decay times of 27.48, 28.87, and 39.82 μs for as-cast, TA, and CN modified devices, respectively. It is noted that the decay time with CN as additive in D18:PY-IT system is intensified distinctly, which implies that CN-treated device provides sufficient time for charge transport in the active layer and ultimately suppresses the internal charge recombination efficiently [48]. Moreover, the TPC test was also carried out at the same device condition, as presented in Fig. 5(f). It is illustrated that the extracted charges under short-circuit state are 2.17 × 10^{-9}, 2.27 × 10^{-9}, and 3.7 × 10^{-9} C for as-cast, TA, and CN modified devices, respectively, where the CN-based device shows the highest extracted charges than other two devices. This obvious enhancement in the extracted charges indicates that the introduction of CN additive can facilitate the charge carrier extraction feasibly, resulting from the optimized phase morphology via synergistic fibrillization between polymer donor and polymer acceptor [49]. In short, the incorporation of CN additive can promote the charges to sweep out from active layer rapidly and thus reduce the internal bimolecular recombination, benefiting for improving photovoltaic performance sufficiently including J_{SC}, FFs, and PCEs.

To investigate the influence of CN additive on the internal ultrafast photogenerated charge dynamics and charge recombination properties in D18:PY-IT system, the transient absorption test was carried out, as displayed in Fig. 6. Here, the excitation wavelength at 800 nm is utilized to only excite polymer acceptor of PY-IT for examining the hole-transfer kinetics in the D18:PY-IT blend films. The two-dimensional (2D) TA spectra of D18:PY-IT films with different treatments under 800 nm excitation were presented in Figs. 6(a)–6(c), while the corresponding curves at various delay times were figured out in Figs. 6(d)–6(f). It is clearly noted that all devices show the obvious ground-state bleach (GSB) signals ranging from 550 to 650 nm, which implies that no absorption is occurred. But there are distinct absorption signals from 660 to 750 nm, ascribing to the photoinduced absorption of singlet excitons from PY-IT acceptor. This phenomenon is a confirmable ultrafast hole transfer from PY-IT to D18 [50]. Also, the kinetics of photoinduced bleaching signals probed at 640 nm were studied, as presented in Fig. S7 in the ESM. It is apparent that the blend film with CN additive shows the fastest rising component with the decreased charge transfer lifetimes from 1.15 ps of as-cast film to 0.73 and 0.46 ps of TA and CN treated blend films, respectively. These results demonstrate that the introduction of CN as additive can speed up hole transfer kinetics, promoting the exciton diffusion and dissociation, and eventually realizing higher photovoltaic performance in all-PSCs.

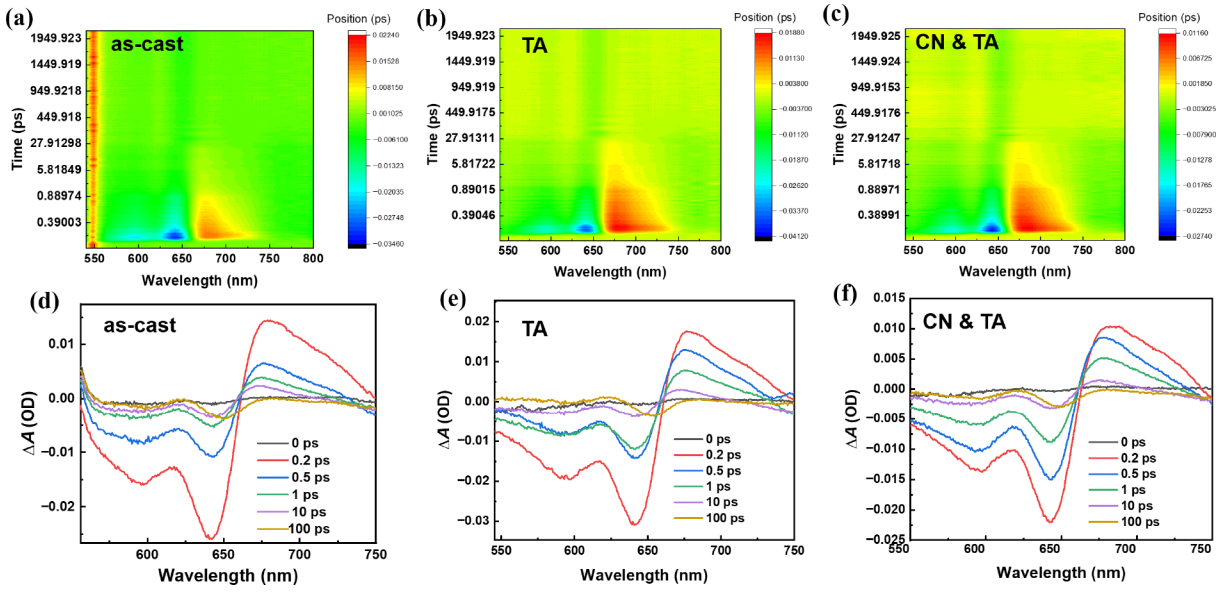

Figure 6 ((a)–(c)) 2D TA spectra under 800 nm excitation and ((d)–(f)) TA spectra at different delay times, for as-cast, TA, and CN-treated D18:PY-IT blend films.

3 Conclusions

To conclude, we utilized CN as a versatile additive to control polymer fibrillization of donor and acceptor synergistically in a D18:PY-IT-based BHJ all-PSCs. Thanks to the introduction of CN additive, the molecular stacking and orientation were improved dramatically, which is preferable to forming face-on stacking patterns. Consequently, the phase purities were elevated between donor and acceptor phases to form the distinguished nano-scale bi-continuous phase separation, resulting in better exciton diffusion and dissociation, and charge transport in the active layer. Furthermore, the incorporation of CN effectively suppressed the charge recombination, leading to higher photovoltaic performance. As a result, the CN-modified all-PSC gave the highest photovoltaic characteristics with a PCE of 17.31%, a V_{OC} of 0.955 V, a J_{SC} of 24.16 mA·cm^{-2}, and an FF of 74.99%, respectively. This PCE is one of the highest values based on reported D18:PY-IT binary BHJ all-PSCs. In addition, this all-PSC exhibited high photovoltaic performance even at a 300 nm-thick D18:PY-IT layer, sustaining 85% efficiency of the initial PCE. Furthermore, the CN-treated device showed a higher stability with a T_{80} lifetime of more than 100 days. These results demonstrate that CN is a good additive for D18:PY-IT based all-PSCs. On the basis of above investigation, it is believed that the appropriate introduction of additives can effectively improve morphology and fibrillization, aiming to realize high-efficiency and stable all-PSCs. Although the incorporation of additive can achieve excellent photovoltaic performance, the morphology control and polymer fibrillization engineering in all-PSCs are complicated and difficult tasks. To achieve more success, we believe that the new development of additives and hybrid treatment will be possibly accessible methodology to optimize device engineering in all-PSCs.

4 Experimental section

4.1 Materials

The solvents and additives of chloroform, methanol (Sigma-Aldrich, ≥ 99%), and CN (Sigma-Aldrich, 98%) were purchased commercially. The HTL of PEDOT:PSS (CLEVIOS P VP AI 4083) was purchased from Heraeus. The polymer acceptor of PY-IT and ETL of PDINN were purchased from Solarmer Material Inc. The polymer donor of D18 was purchased from Derthon Optoelectronics Materials Science Technology Co. Ltd. In this study, all of solvents, additives, and materials were used as received without further purification.

4.2 Device fabrication

In this work, the conventional device architecture of ITO/PEDOT:PSS/active layer/PDINN/Ag was utilized directly [51, 52]. Firstly, ITO substrates were cleaned sequentially with surfactant aqueous solution, deionized water, and isopropanol under continuous ultrasonic treatment for 15 min each, followed by drying ITO substrates in an 80 °C oven for 2 h. After UV–ozone treatment for 3 min on ITO substrates, PEDOT:PSS layer was spin-coated on ITO at 4000 rpm for 30 s (40 nm). Subsequently, the substrates covered with PEDOT:PSS were annealed at 150 °C in ambient for another 15 min. The annealed substrates were then transferred to a nitrogen-filled glove box for spin-coating active layer. The preparation of active layer solution was as follows: D18:PY-IT (weight ratio of 1:1.1 in chloroform with a total concentration of 10 mg·mL^{-1}) was stirred at room temperature for 3 h and then stirred at 100 °C for another 30 min. Then, the additive of CN (0.25%) was added to the active layer solution approximately 30 min before spin-coating. The active layer was spin coated at 2000 rpm for 30 s (110 nm) and then annealed at 100 °C for 10 min. Next, the ETL of PDINN solution (1 mg·mL^{-1} in methanol) was spin-coated at 3000 rpm for 30 s (10 nm). At last, a 100 nm thickness of Ag electrode was thermally evaporated through a mask (effective area of 0.057 cm^2) under a vacuum of about 4×10^{-4} mbar.

Electronic Supplementary Material: Supplementary material (including characterization, *J*–*V* and EQE curves of different CN concentration and different thickness of active layer, AFM image, electron and hole mobilities, kinetic curves of photoinduced bleaching signals, and data summary) is available in the online version of this article at https://doi.org/10.26599/NR.2025.94907295.

Data availability

All data needed to support the conclusions in the paper are presented in the manuscript and the Electronic Supplementary Material. Additional data related to this paper may be requested from the corresponding author upon request.

Acknowledgements

This work was supported by the National Natural Science Foundation of China (No. 52373175), Guizhou Provincial Basic Research Program (General Program) (No. zk[2025]603), the High-level Innovative Talents Foundation of Guizhou Province (No. QKHPTRC-GCC[2023]024), Natural Science Foundation of Guizhou Province (No. QKHPTRC-CXTD[2023]005), Science and Technology Innovation Team of Higher Education Department of Guizhou Province (No. QJJ[2023]053), Natural Science Foundation of Guizhou University (No. GZUTGH[2023]12), and Science and Technology Innovation Team of Guizhou University (No. GZUKCT[2023]01). L. M. D. thanks the National Key Research and Development Program of China (Nos. 2022YFB3803300 and 2023YFE0116800) and Beijing Natural Science Foundation (No. IS23037).

Declaration of competing interest

All the contributing authors report no conflict of interests in this work.

Author contribution statement

B. Z.: Writing manuscript, writing – review & editing, supervision, project administration, formal analysis, data curation, conceptualization. Y. S. Z.: Methodology, investigation, formal analysis, data curation. X. F. Q.: Methodology, formal analysis. A. Q. L.: Methodology. X. L. L.: Methodology. W. M. L.: Formal analysis. W. L. G.: Formal analysis. X. L. Q.: Formal analysis. Z. C. H.: Resources, methodology, investigation, formal analysis. Y. H.: Resources, formal analysis. M. L. L.: Writing – editing, resources, supervision, project administration, formal analysis. L. M. D.: Writing – editing, supervision, project administration, formal analysis. All the authors have approved the final manuscript.

Use of AI statement

None.

References

[1] Wu, M. H.; Ma, B.; Li, S. S.; Han, J. Q.; Zhao, W. C. Powering the future: A critical review of research progress in enhancing stability of high‐efficiency organic solar cells. *Adv. Funct. Mater.* **2023**, *33*, 2305445.

[2] Chen, C.; Wang, L.; Xia, W. Y.; Qiu, K.; Guo, C. H.; Gan, Z. R.; Zhou, J.; Sun, Y. D.; Liu, D.; Li, W. et al. Molecular interaction induced dual fibrils towards organic solar cells with certified efficiency over 20%. *Nat. Commun.* **2024**, *15*, 6865.

[3] Wei, N.; Chen, J. N.; Cheng, Y. T.; Bian, Z. Q.; Liu, W. L.; Song, H. M.; Guo, Y. W.; Zhang, W. K.; Liu, Y. H.; Lu, H. et al. Constructing multiscale fibrous morphology to achieve 20% efficiency organic solar cells by mixing high and low molecular weight D18. *Adv. Mater.* **2024**, *36*, 2408934.

[4] Chen, Z. Y.; Ge, J. F.; Song, W.; Tong, X. Y.; Liu, H.; Yu, X. L.; Li, J.; Shi, J. Y.; Xie, L.; Han, C. C. et al. 20.2% efficiency organic photovoltaics employing a π-extension quinoxaline-based acceptor with ordered arrangement. *Adv. Mater.* **2024**, *36*, 2406690.

[5] Guan, S. T.; Li, Y. K.; Xu, C.; Yin, N.; Xu, C. R.; Wang, C. X.; Wang, M. T.; Xu, Y. X.; Chen, Q.; Wang, D. W. et al. Self-assembled interlayer enables high-performance organic photovoltaics with power conversion efficiency exceeding 20%. *Adv. Mater.* **2024**, *36*, 2400342.

[6] Thompson, B. C.; Fréchet, J. M. J. Polymer-fullerene composite solar cells. *Angew. Chem., Int. Ed.* **2008**, *47*, 58–77.

[7] Jørgensen, M.; Norrman, K.; Gevorgyan, S. A.; Tromholt, T.; Andreasen, B.; Krebs, F. C. Stability of polymer solar cells. *Adv. Mater.* **2012**, *24*, 580–612.

[8] Günes, S.; Neugebauer, H.; Sariciftci, N. S. Conjugated polymer-based organic solar cells. *Chem. Rev.* **2007**, *107*, 1324–1338.

[9] Liu, Q. S.; Jiang, Y. F.; Jin, K.; Qin, J. Q.; Xu, J. G.; Li, W. T.; Xiong, J.; Liu, J. F.; Xiao, Z.; Sun, K. et al. 18% Efficiency organic solar cells. *Sci. Bull.* **2020**, *65*, 272–275.

[10] Qin, J. Q.; Zhang, L. X.; Zuo, C. T.; Xiao, Z.; Yuan, Y. B.; Yang, S. F.; Hao, F.; Cheng, M.; Sun, K.; Bao, Q. Y. et al. A chlorinated copolymer donor demonstrates a 18.13% power conversion efficiency. *J. Semicond.* **2021**, *42*, 010501.

[11] Meng, X. Y.; Jin, K.; Xiao, Z.; Ding, L. M. Side chain engineering on D18 polymers yields 18.74% power conversion efficiency. *J. Semicond.* **2021**, *42*, 100501.

[12] Zhang, M. J.; Guo, X.; Ma, W.; Ade, H.; Hou, J. H. A large-bandgap conjugated polymer for versatile photovoltaic applications with high performance. *Adv. Mater.* **2015**, *27*, 4655–4660.

[13] Yuan, J.; Zhang, Y. Q.; Zhou, L. Y.; Zhang, G. C.; Yip, H. L.; Lau, T. K.; Lu, X. H.; Zhu, C.; Peng, H. J.; Johnson, P. A. et al. Single-junction organic solar cell with over 15% efficiency using fused-ring acceptor with electron-deficient core. *Joule* **2019**, *3*, 1140–1151.

[14] Song, J. L.; Zhu, L.; Li, C.; Xu, J. Q.; Wu, H. B.; Zhang, X. N.; Zhang, Y.; Tang, Z.; Liu, F.; Sun, Y. M. High-efficiency organic solar cells with low voltage loss induced by solvent additive strategy. *Matter* **2021**, *4*, 2542–2552.

[15] Cui, Y.; Yao, H. F.; Zhang, J. Q.; Xian, K. H.; Zhang, T.; Hong, L.; Wang, Y. M.; Xu, Y.; Ma, K. Q.; An, C. B. et al. Single-junction organic photovoltaic cells with approaching 18% efficiency. *Adv. Mater.* **2020**, *32*, 1908205.

[16] Wang, W.; Wu, Q.; Sun, R.; Guo, J.; Wu, Y.; Shi, M. M.; Yang, W. Y.; Li, H. N.; Min, J. Controlling molecular mass of low-band-gap polymer acceptors for high-performance all-polymer solar cells. *Joule* **2020**, *4*, 1070–1086.

[17] Luo, Z. H.; Liu, T.; Ma, R. J.; Xiao, Y. Q.; Zhan, L. L.; Zhang, G. Y.; Sun, H. L.; Ni, F.; Chai, G. D.; Wang, J. W. et al. Precisely controlling the position of bromine on the end group enables well-regular polymer acceptors for all-polymer solar cells with efficiencies over 15%. *Adv. Mater.* **2020**, *32*, 2005942.

[18] Wu, B. Q.; Zhang, Y.; Tian, S. Z.; Oh, J.; Yang, M. Q.; Pan, L. H.; Yin, B. Y.; Yang, C.; Duan, C. H.; Huang, F. et al. Non-fused polymerized small molecular acceptors for efficient all-polymer solar cells. *Sol. RRL* **2022**, *6*, 2101034.

[19] Wu, B. Q.; Li, Y. L.; Liu, K. Z.; Kim, S.; Yuan, X. Y.; Pan, L. H.; Zhou, X.; Tian, S. Z.; Yang, C.; Huang, F. et al. An asymmetric polymerized small molecular acceptor with temperature-dependent aggregation and superior batch-to-batch reproducibility for efficient all-polymer solar cells. *Nano Energy* **2024**, *128*, 109874.

[20] Zhang, L.; Jia, T.; Pan, L. H.; Wu, B. Q.; Wang, Z. Y.; Gao, K.; Liu, F.; Duan, C. H.; Huang, F.; Cao, Y. 15.4% Efficiency all-polymer solar cells. *Sci. China Chem.* **2021**, *64*, 408–412.

[21] Zhang, B.; Zhao, Y. S.; Xu, C. D.; Feng, C.; Li, W. M.; Qin, X. F.; Lv, M. L.; Luo, X. Y.; Qin, X. L.; Li, A. Q. et al. Perylene diimide-based low-cost and thickness-tolerant electron transport layer enables polymer solar cells approaching 19% efficiency. *Adv. Funct. Mater.* **2024**, *34*, 2400903.

[22] Facchetti, A. Polymer donor–polymer acceptor (all-polymer) solar cells. *Mater. Today* **2013**, *16*, 123–132.

[23] Wu, B. Q.; Yin, B. Y.; Duan, C. H.; Ding, L. M. All-polymer solar cells. *J. Semicond.* **2021**, *42*, 080301.
[24] Song, J. L.; Li, C.; Ma, H. S.; Han, B. Y.; Wang, Q. Q.; Wang, X. C.; Wei, D. H.; Bu, L. J.; Yang, R. Q.; Yan, H. et al. Optimizing double-fibril network morphology via solid additive strategy enables binary all-polymer solar cells with 19.50% efficiency. *Adv. Mater.* **2024**, *36*, 2406922.
[25] Chen, T. Q.; Zhong, Y. Y.; Duan, T. N.; Tang, X.; Zhao, W. K.; Wang, J. Y.; Lu, G. H.; Long, G. K.; Zhang, J. B.; Han, K. et al. Asymmetrified benzothiadiazole-based solid additives enable all-polymer solar cells with efficiency over 19%. *Angew. Chem.* **2025**, *137*, e202412983.
[26] Wang, Z. T.; Wang, X.; Tu, L. J.; Wang, H.; Du, M. Z.; Dai, T. T.; Guo, Q.; Shi, Y. Q.; Zhou, E. J. Dithienoquinoxalineimide-based polymer donor enables all-polymer solar cells over 19% efficiency. *Angew. Chem., Int. Ed.* **2024**, *63*, e202319755.
[27] Kang, H.; Lee, W.; Oh, J.; Kim, T.; Lee, C.; Kim, B. J. From fullerene-polymer to all-polymer solar cells: The importance of molecular packing, orientation, and morphology control. *Acc. Chem. Res.* **2016**, *49*, 2424–2434.
[28] Zhao, Y. S.; Wu, J. Y.; Li, W. M.; Qin, X. F.; Lv, M. L.; Hua, Y.; Zhu, W. G.; He, Z. C.; Zhang, B. Morphology control realizes fast charge dissociation and transport in high-performance all-polymer solar cells. *ACS Appl. Energy Mater.* **2024**, *7*, 4180–4189.
[29] Cheng, C.; Wu, Y. L.; Cendra, C.; Schneider, S.; Treiber, J.; Agarwala, P.; Gomez, E. D.; Bao, Z. N.; Takacs, C.; Toney, M. F. et al. Impact of dilute DIO additive on local microstructure of fluorinated, pNDI-based polymer solar cells. *Adv. Mater.* **2024**, *36*, 2409502.
[30] Miao, Y. W.; Sun, Y. N.; Zou, W. T.; Zhang, X.; Kan, Y. Y.; Zhang, W. Q.; Jiang, X. Y.; Wang, X. C.; Yang, R. Q.; Hao, X. T. et al. Isomerization engineering of solid additives enables highly efficient organic solar cells via manipulating molecular stacking and aggregation of active layer. *Adv. Mater.* **2024**, *36*, 2406623.
[31] Feng, W. Y.; Chen, T. Q.; Li, Y. L.; Duan, T. N.; Jiang, X.; Zhong, C.; Zhang, Y. X.; Yu, J. F.; Lu, G. H.; Wan, X. J. et al. Binary all-polymer solar cells with a perhalogenated-thiophene-based solid additive surpass 18% efficiency. *Angew. Chem., Int. Ed.* **2024**, *63*, e202316698.
[32] Zhang, Y.; Wu, B. Q.; He, Y. K.; Deng, W. Y.; Li, J. W.; Li, J. Y.; Qiao, N.; Xing, Y. F.; Yuan, X. Y.; Li, N. et al. Layer-by-layer processed binary all-polymer solar cells with efficiency over 16% enabled by finely optimized morphology. *Nano Energy* **2022**, *93*, 106858.
[33] Li, Z. Y.; Liang, Y. F.; Qian, X. T.; Ying, L.; Cao, Y. Suppressing non-radiative loss via a low-cost solvent additive enables high-stable all-polymer solar cells with 16.13% efficiency. *Chem. Eng. J.* **2022**, *446*, 136877.
[34] Sheng, H.; Liu, S. Z.; Kang, X.; Niu, J. N.; Adewale, A. A.; Wen, S. G.; Yang, C. M.; Bao, X. C.; Sun, M. L. A benzobisoxazole-based polymer assisting high efficiency polymer solar cells. *Nano Energy* **2024**, *126*, 109648.
[35] Zhang, W. Q.; Sun, C. K.; Angunawela, I.; Meng, L.; Qin, S. C.; Zhou, L. Y.; Li, S. M.; Zhuo, H. M.; Yang, G.; Zhang, Z. G. et al. 16.52% efficiency all-polymer solar cells with high tolerance of the photoactive layer thickness. *Adv. Mater.* **2022**, *34*, 2108749.
[36] Shen, Y. F.; Zhang, J. Q.; Tian, C. Y.; Qiu, D. D.; Wei, Z. X. Slot-die coated large-area flexible all-polymer solar cells by non-halogenated solvent. *Nano Res.* **2023**, *16*, 13008–13013.
[37] Mahmood, A.; Wang, J. L. A review of grazing incidence small- and wide-angle X-ray scattering techniques for exploring the film morphology of organic solar cells. *Sol. RRL* **2020**, *4*, 2000337.
[38] Li, D. H.; Deng, N.; Fu, Y. W.; Guo, C. H.; Zhou, B. J.; Wang, L.; Zhou, J.; Liu, D.; Li, W.; Wang, K. et al. Fibrillization of non-fullerene acceptors enables 19% efficiency pseudo-bulk heterojunction organic solar cells. *Adv. Mater.* **2023**, *35*, 2208211.
[39] Zhu, L.; Zhang, M.; Xu, J. Q.; Li, C.; Yan, J.; Zhou, G. Q.; Zhong, W. K.; Hao, T. Y.; Song, J. L.; Xue, X. N. et al. Single-junction organic solar cells with over 19% efficiency enabled by a refined double-fibril network morphology. *Nat. Mater.* **2022**, *21*, 656–663.
[40] Liu, X.; Zhang, C. H.; Duan, C. H.; Li, M. M.; Hu, Z. C.; Wang, J.; Liu, F.; Li, N.; Brabec, C. J.; Janssen, R. A. J. et al. Morphology optimization via side chain engineering enables all-polymer solar cells with excellent fill factor and stability. *J. Am. Chem. Soc.* **2018**, *140*, 8934–8943.
[41] He, C. L.; Pan, Y. W.; Ouyang, Y. N.; Shen, Q.; Gao, Y.; Yan, K. R.; Fang, J.; Chen, Y. Y.; Ma, C. Q.; Min, J. et al. Manipulating the D:A interfacial energetics and intermolecular packing for 19.2% efficiency organic photovoltaics. *Energy Environ. Sci.* **2022**, *15*, 2537–2544.
[42] Chen, Q. L.; Huang, H.; Hu, D.; Zhang, C.; Xu, X. J.; Lu, H.; Wu, Y. G.; Yang, C. L.; Bo, Z. S. Improving the performance of layer-by-layer processed organic solar cells via introducing a wide-bandgap dopant into the upper acceptor layer. *Adv. Mater.* **2023**, *35*, 2211372.
[43] Wang, X. J.; Yi, S. W.; He, Z. C.; Ouyang, X. H.; Wu, H. B.; Zhu, W. G.; Zhang, B.; Cao, Y. An environmentally friendly natural polymer as a universal interfacial modifier for fullerene and non-fullerene polymer solar cells. *Sustain. Energ. Fuels* **2020**, *4*, 1234–1241.
[44] Feng, H. R.; Dai, Y.; Guo, L. H.; Wang, D.; Dong, H.; Liu, Z. H.; Zhang, L.; Zhu, Y.; Su, C.; Chen, Y. S. et al. Exploring ternary organic photovoltaics for the reduced nonradiative recombination and improved efficiency over 17.23% with a simple large-bandgap small molecular third component. *Nano Res.* **2022**, *15*, 3222–3229.
[45] MacKenzie, R. C. I.; Shuttle, C. G.; Chabinyc, M. L.; Nelson, J. Extracting microscopic device parameters from transient photocurrent measurements of P3HT:PCBM solar cells. *Adv. Energy Mater.* **2012**, *2*, 662–669.
[46] Street, R. A. Localized state distribution and its effect on recombination in organic solar cells. *Phys. Rev. B* **2011**, *84*, 075208.
[47] Sae-Kung, C.; Wright, B. F.; Clarke, T. M.; Wallace, G. G.; Mozer, A. J. Effects of interfacial layers on the open circuit voltage of polymer/fullerene bulk heterojunction devices studied by charge extraction techniques. *ACS Appl. Mater. Interfaces* **2019**, *11*, 21030–21041.
[48] Wu, Z. H.; Sun, C.; Dong, S.; Jiang, X. F.; Wu, S. P.; Wu, H. B.; Yip, H. L.; Huang, F.; Cao, Y. n-Type water/alcohol-soluble naphthalene diimide-based conjugated polymers for high-performance polymer solar cells. *J. Am. Chem. Soc.* **2016**, *138*, 2004–2013.
[49] Ma, R. J.; Zhou, K. K.; Sun, Y. N.; Liu, T.; Kan, Y. Y.; Xiao, Y. Q.; Peña, T. A. D.; Li, Y. X.; Zou, X. H.; Xing, Z. S. et al. Achieving high efficiency and well-kept ductility in ternary all-polymer organic photovoltaic blends thanks to two well miscible donors. *Matter* **2022**, *5*, 725–734.
[50] Zhang, T.; Xu, Y.; Yao, H. F.; Zhang, J. Q.; Bi, P. Q.; Chen, Z. H.; Wang, J. W.; Cui, Y.; Ma, L. J.; Xian, K. H. et al. Suppressing the energetic disorder of all-polymer solar cells enables over 18% efficiency. *Energy Environ. Sci.* **2023**, *16*, 1581–1589.
[51] Sun, Y. N.; Nian, L.; Kan, Y. Y.; Ren, Y.; Chen, Z. H.; Zhu, L.; Zhang, M.; Yin, H.; Xu, H. J.; Li, J. F. et al. Rational control of sequential morphology evolution and vertical distribution toward 17.18% efficiency all-small-molecule organic solar cells. *Joule* **2022**, *6*, 2835–2848.
[52] Kan, Y. Y.; Sun, Y. N.; Ren, Y.; Xu, Y. X.; Jiang, X. Y.; Shen, H. J.; Geng, L. L.; Li, J. F.; Cai, P.; Xu, H. J. et al. Amino-functionalized graphdiyne derivative as a cathode interface layer with high thickness tolerance for highly efficient organic solar cells. *Adv. Mater.* **2024**, *36*, 2312635.